optica

Asymmetric single-cycle control of valence electron motion in polar chemical bonds

Yuya Morimoto,[1,2,3,*,†] Yasushi Shinohara,[4,5,†] Mizuki Tani,[5] Bo-Han Chen,[1,2,6] Kenichi L. Ishikawa,[4,5,7] and Peter Baum[1,2,6]

[1]Ludwig-Maximilians-Universität München, Am Coulombwall 1, 85748 Garching, Germany
[2]Max-Planck-Institute of Quantum Optics, Hans-Kopfermann-Str. 1, 85748 Garching, Germany
[3]Current Address: Friedrich-Alexander-Universität Erlangen-Nürnberg, Staudtstraße 1, 91058, Erlangen, Germany
[4]Photon Science Center, Graduate School of Engineering, The University of Tokyo, 7-3-1 Hongo, Bunkyo-ku, Tokyo 113-8656, Japan
[5]Department of Nuclear Engineering and Management, Graduate School of Engineering, The University of Tokyo, 7-3-1 Hongo, Bunkyo-ku, Tokyo 113-8656, Japan
[6]University of Konstanz, Universitätsstraße 10, 78457 Konstanz, Germany
[7]Research Institute for Photon Science and Laser Technology, The University of Tokyo, 7-3-1 Hongo, Bunkyo-ku, Tokyo 113-0033, Japan
*Corresponding author: yuya.morimoto@fau.de

Received 4 November 2020; revised 22 December 2020; accepted 26 January 2021 (Doc. ID 414213); published 12 March 2021

A dielectric material's response to light is microscopically defined by field-cycle-driven motion of electron densities in the restoring forces of the atomic environment. Here we apply single-cycle mid-infrared pulses to drive the nonlinear motion of valence electrons in a heteronuclear crystal with asymmetric structure and report how the macroscopic optical response can be tracked back to the real-space electron dynamics in the symmetry-breaking potential along the chemical bonds. Whether our single-cycle field drives electrons from the less electronegative to the more electronegative element or vice versa controls the appearance of a smooth nonlinear output spectrum or one with even and odd harmonic orders. Crystal angle scans reveal the absolute orientation of the asymmetric bonds. Directional motion of valence charges controlled by a single cycle of light can therefore be used for spectroscopically exploring the binding potential, to understand and design novel materials for nonlinear optics, or to eventually process information at the frequency of light.

https://doi.org/10.1364/OPTICA.414213

1. INTRODUCTION

When a light wave interacts with a transparent material, such as gas-phase atoms, molecules, liquid, or a dielectric solid, electron densities are driven by the electric field of the optical cycles and move in the restoring forces of the atomic environment. Based on the complexity of this interaction in the nonlinear and strong-field regimes [1–9], researchers are exploring the possibility of electronics and information processing at the frequency of light [10–18] via controlling electronic motion on level of the optical field cycles [19–21]. Materials for cycle-based nonlinear optics and information processing should have low absorption losses, a complex potential energy landscape, and a direct nonlinear response to single-cycle excitation. Researchers also aim at reconstructing the band structure and the potential of a crystalline material by all-optical nonlinear spectroscopy [22–24]. For both objectives, and for comprehending the foundations of nonlinear optics, we need to understand the nonlinear response of a complex material to an impulsive single-cycle excitation and determine the relevant connections to the atomic structure.

Sub-cycle and single-cycle pulses have been reported to trigger broadband high-frequency light emission from symmetric or isotropic media such as rare gas atoms [25], nanocrystalline dielectrics [10,18], or semiconductors [26,27] in form of isolated short-wavelength light pulses, forming the foundation of attosecond science [28]. In parallel, directional nonlinear optics in asymmetric materials were reported [29–32], for example, by Frumker and Corkum *et al.* [33,34] and Wörner *et al.* [35] in oriented molecules, and by Huber *et al.* in a GaSe crystal on basis of few-cycle excitation and time-domain characterization [16,17]. The connecting question, whether a single cycle of light can launch an isolated, unidirectional electronic motion in a material with a network of asymmetric, oriented chemical bonds and how such dynamics can be tracked by spectroscopy, is the focus of this report.

We excite a two-dimensional (2D) layered crystal of ε-GaSe and its heterogeneous chemical bonds with octave-spanning near-single-cycle pulses of mid-infrared light and relate the resulting quasi-ballistic, coherent electronic motion to the direction and polarity of the bonds. The excitation with only one relevant optical cycle produces approximately the optical impulse response in time as functions of electric field directions and bond orientations. The experiment, therefore, explores the physics of isolated single-cycle excitation [10,26,27] in a material with symmetry-breaking nonlinear response [16,17], thus connecting crystallography on the level of the chemical bonds with optics on the level of a single cycle of light. In contrast to previous experiments with longer pulses

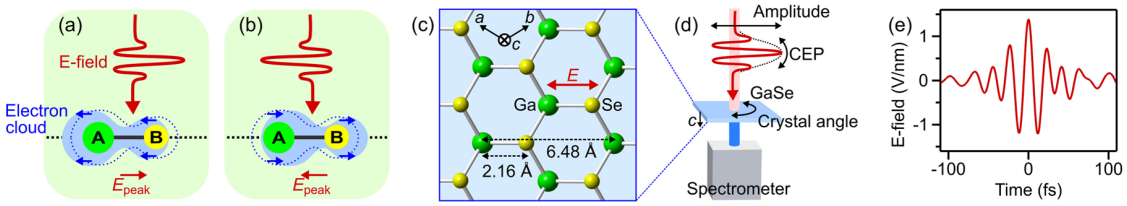

Fig. 1. Concept and experiment. (a), (b) An asymmetric chemical bond (solid line) in a crystal is excited by a single-cycle laser pulse (red). Depending on the direction of the most intense electric field cycle (E_{peak}), electron density (blue) is coherently driven along or opposite to the polarity of the bond (atoms A and B). The field-driven electrons emit new light with a waveform determined by the atoms' electronegativity. (c) Crystal structure of one monolayer of ε-GaSe crystal in the $a-b$ plane. (d) Experiment. Near-single-cycle mid-infrared laser pulse (red) is focused into a ε-GaSe crystal (blue), and the output spectrum is analyzed as a function of crystal angle and peak field direction. (e) Electric field of the driving pulse in the experiment.

[16,17], the shape of the nonlinear output spectrum is directly related to the absolute orientation of the chemical bonds, and no measurements in time domain are required to understand the basics of the nonlinear response of valence electrons in real space.

2. RESULTS AND DISCUSSION

A. Experimental Results

The experiment is depicted in Fig. 1(d). A near-single-cycle optical pulse [1.6 cycle FWHM; see Fig. 1(e)] with a central frequency of 43 THz (7 μm wavelength) is obtained via optical parametric amplification [36] and focused into a 21-μm-thick single crystal of gallium selenide (ε-GaSe). The optical spectrum does not excite any infrared active phonon modes [37], and the photon energy of ∼0.18 eV is far below the bandgap of 2.0 eV [38]. The peak field strength inside the crystal is 1.4 V/nm, and the electric field is parallel to the Ga–Se bonds in the $a-b$ plane [Fig. 1(c)]; see also Supplement 1. The nonlinear optical interaction inside the crystal generates higher-frequency radiation that is mostly polarized parallel to the driving field [15,39]. The output photons are collected with a silver-coated spherical mirror (50 mm focal length) and guided via an InF_3 multimode fiber (Le Verre Fluoré) into three types of spectrometers, namely a Fourier transform spectrometer (L-FTS, LASNIX) for the mid-infrared range, a grating-based spectrometer with a InGaAs detector for the near-infrared range (Rock NIR RSM-445, Ibsen Photonics), and a spectrograph with a silicon detector for visible light (USB-2000+, Ocean Optics). These spectrometers have calibrated sensitivities and overlapping spectral ranges that allow us to determine a concatenated result [15].

Figure 2(a) shows the observed output spectra from the GaSe crystal as a function of the excitation pulse's carrier-envelope phase (CEP, φ_{CE}). We see a broadband nonlinear light emission that ranges from the fundamental frequency (43 THz, $\lambda = 7.0$ μm) to a more than 17-fold higher frequency of more than 750 THz ($\lambda = 0.4$ μm); the optical fiber absorbs the light beyond that range. Depending on the CEP, the spectrum consists of a pronounced sequence of harmonic orders ($\varphi_{CE} = \pi = 180°$) or alternatively covers smoothly the whole range without interferences [10,26,27]. A common peak around 480 THz is incoherent photoluminescence (PL) at the bandgap of ∼2 eV from residual nonlinear absorption. In Figs. 2(b) and 2(c), we show the spectral details at two special CEP values, $\varphi_{CE} = 0$ and $\varphi_{CE} = \pi = 180°$, the white lines in Fig. 2(a). At these values, the temporal excitation waveforms are identical and have a single optical cycle that is most intense, but the absolute direction of the electric field is flipped. We call $\varphi_{CE} = 0$ a cosine excitation and $\varphi_{CE} = \pi$ a minus-cosine excitation. At $\varphi_{CE} = 0$, the spectrum is smooth, while at $\varphi_{CE} = \pi$ the spectrum shows a set of distinct harmonic peaks at a visibility of more than 100. There are even-order and odd-order harmonics with a spacing given by one photon energy of the driving frequency (43 THz, 0.18 eV). Usually, a harmonic spectrum [15–17] or a smooth spectrum [10,26,27] is observed with multi-cycle or single-cycle excitation, respectively. The measured switch by simply flipping the electric field direction of a single-cycle excitation therefore indicates a potentially novel regime of interaction.

B. Real-Space Explanation

In order to understand the field-driven electronic motion behind our observations, we refer to earlier works on ε-GaSe by Hohenleutner *et al.* [16] and Langer *et al.* [17] and recall the crystal structure of ε-GaSe as shown in Fig. 1(c); see also Fig. S2 in Supplement 1. The crystal is composed of quasi-2D monolayers that are bonded to each other with van der Waals forces. Our driving electric field oscillates in the $a-b$ plane [see Fig. 1(c)] and inter-layer electron dynamics along the c axis can, therefore, be neglected [17]. An electric pump field vector in the $a-b$ plane will predominantly project only onto one of the three available Ga–Se bonds [see Figs. 1(c) and S2] while the other two bonds at 60 deg bond angles in the $a-b$ plane will see an effectively much weaker projection of the electric field; see Supplement 1 for details. The absolute orientation of all Ga–Se bonds is, hence, unique in ε-GaSe throughout all of the unit cell, and there are no opposite Se–Ga bonds excited. We, therefore, concentrate our analysis on the real-space dynamics of a single polar chemical bond under single-cycle excitation, aiming at an explanation of the phenomenon rather than a quantitative reproduction of the measurement results.

We first apply the simplest possible textbook classical model [1] to our single-cycle excitation. The coupled dynamics of all the electrons and holes driven along the Ga–Se bond direction in the restoring forces of an asymmetric atomic potential is described by a single generalized coordinate of a classical point charge of $-e$ (elementary charge) and mass of m_e (electron rest mass) that moves one-dimensionally on an effective potential $U(\tilde{x})$, where the generalized coordinate $\tilde{x}$ represents the displacement from the equilibrium position; see Fig. 3(a). The effective potential is described by a series of polynomials [1], $U(\tilde{x}) = \sum_{n=2}^{\infty} c_n \tilde{x}^n$, where c_2 gives the linear optical response (as in the Lorentz oscillator model [1]) and c_n ($n > 2$) describes the nonlinearity in the motion of the charge; the odd-order terms determine the asymmetry of the potential. We determine c_2 from the direct bandgap

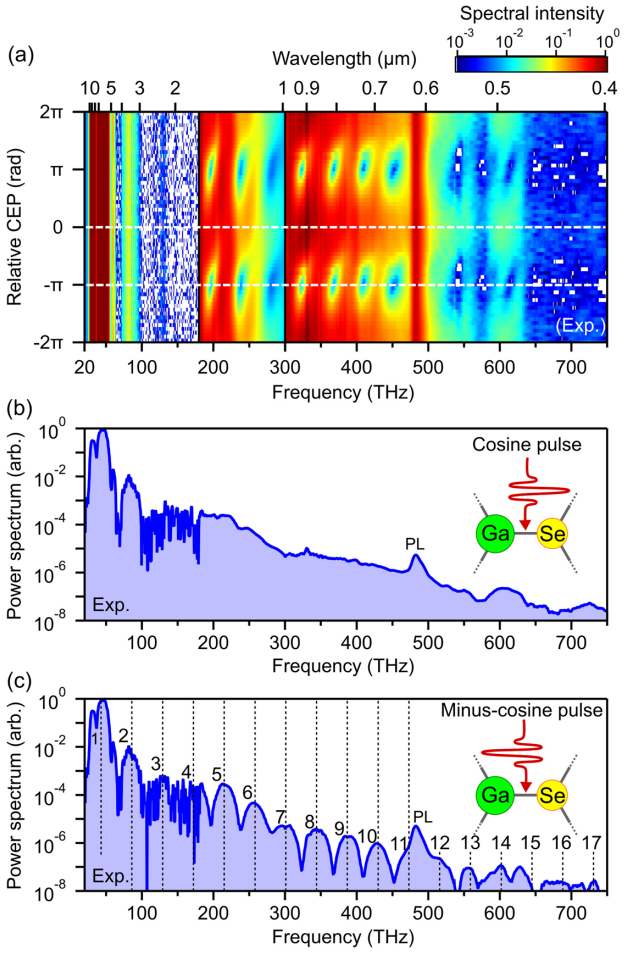

Fig. 2. Experimental results. (a) Observed output spectra as a function of the carrier-envelope phase (CEP) and polarity of the driving field. (b) Experimental output spectrum with cosine excitation (peak field from Ga to Se). (c) Experimental output spectrum with minus-cosine excitation (peak field from Se to Ga).

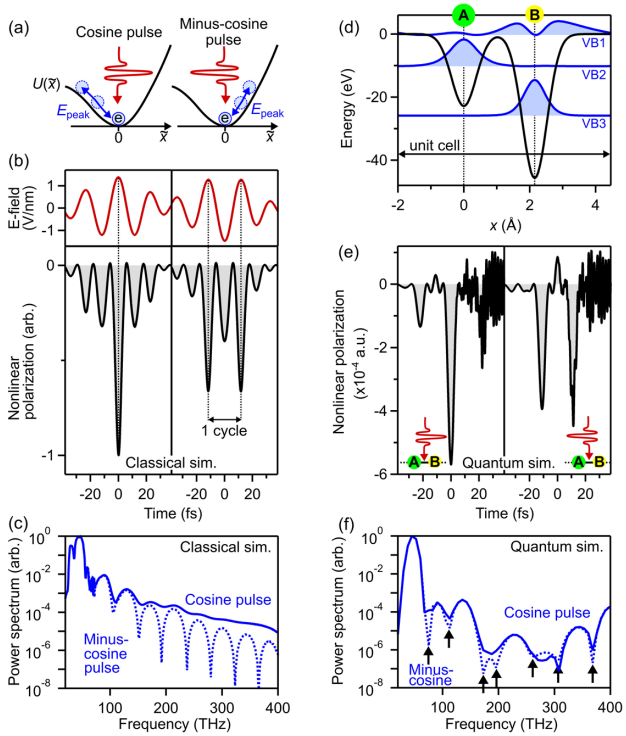

Fig. 3. Real-space explanation. (a) Concept of classical 1D anharmonic oscillator model. The field-driven electronic motion is represented by a classical charged particle (blue) driven by a laser field (red) in an asymmetric potential. (b) Time-dependent nonlinear polarization (black) produced by the laser waveforms (red) as predicted by the classical model. (c) Simulated output spectra from the classical simulation for cosine excitation (solid blue curve) and minus-cosine excitation (dashed blue line). (d) Model potential for the non-perturbative 1D quantum simulation (black) and electron density of the occupied valence bands (blue). (e) Nonlinear polarization from the quantum simulation. Fast oscillations at large times are due to residual nonlinear absorption. (f) Simulated output spectra from the quantum-mechanical model for the cosine driving pulse (solid blue curve) and minus-cosine pulse (dashed blue line). The dip positions (arrows) are not exactly between the harmonic orders because the energy of maximum destructive interference is shifted by the unequal intensities of neighboring harmonics.

and $c_3 - c_6$ from the harmonic intensities in Fig. 2(c); higher orders are neglected. The measured electric field of the single-cycle pulses [see Fig. 1(e)] drives an almost impulsive excitation of real-space motion of the charge. Fourier transformation of the acceleration gives the output spectrum; see Supplement 1 for more details.

Figure 3(c) shows the results for $\varphi_{CE} = 0$ and $\varphi_{CE} = \pi$. Both simulated spectra reproduce nearly all the observed features in the experiment and in particular the appearance and disappearance of the modulation into harmonic orders when changing from a cosine to a minus-cosine excitation field. In order to elucidate the underlying physics, we plot in Fig. 3(b) the nonlinear polarization in the time domain. For a cosine-shaped excitation waveform with a peak toward the steeper potential gradient [left panel in Fig. 3(a)], the nonlinear polarization is predominantly induced only once, at the driving laser's highest field peak. Such an isolated burst of nonlinear polarization corresponds in the spectrum to a broadband, featureless emission like that observed in the experiment of Fig. 2(b). In contrast, a minus-cosine driving pulse [right panel in Fig. 3(a)] with peak field toward the shallower side of the potential produces substantially weaker (~40%) nonlinear polarization at the peak time but instead two emission bursts at the times of the two second-most intense field cycles in opposite direction. These insights are consistent with pioneering experiments and theory on ε-GaSe under multi-cycle excitation, where the spectrum is always modulated at harmonic orders and only the timing of the emission bursts changes with φ_{CE} as a consequence of interferences between odd and even harmonics [16,17].

The above classical model well reproduces the observed spectra (see also Fig. S5 in Supplement 1) but lacks the directionality of the asymmetric bonds and various potential influences of quantum-mechanical effects (see below). In an almost equally simple, but quantum-mechanical model, we consider real-space electron dynamics in a one-dimensional (1D) model crystal whose unit cell is composed of two different atoms A and B [see Figs. 1(a) and 1(b)] in periodic arrangement. This choice is motivated by drawing a straight line through GaSe along one of the bonds [see Fig. 1(c)]. We refrain from quantitatively reproducing the observed spectra with more elaborate theories—for example, semiconductor Bloch equations [40,41] or time-dependent density functional theory [41–43]—but rather attempt to grasp an essential and instructive real-space picture of impulsively driven electronic motion under consideration of quantum effects such as Bragg reflection and

kinetic energy shift due to the intraband motion. Atom A has lower electron affinity and corresponds to Ga while atom B has a larger electron affinity and corresponds to Se. We choose a unit cell size of $a = 12.2$ au $= 6.5$ Å and atom positions at $x_A = a/3$ and $x_B = 2a/3$, compared with Fig. 1(c). The black line in Fig. 3(d) shows the real-space potential for this asymmetric system; the depths of the two atomic potentials are chosen to reproduce the direct bandgap of ε-GaSe of 2.0 eV [38]. The corresponding band structure is shown in Fig. S6(a) in Supplement 1. Before the interaction with the laser, we populate the three lowest bands (VB1 to VB3) with six electrons per unit cell, in order to mimic the electronic structure of three-dimensional ε-GaSe [44] where the valence electrons are predominantly localized around the nuclei and the electrons of VB1 are mostly on Se [45]. The corresponding ground-state electron densities are depicted in Fig. 3(d) in blue (see also Fig. S6(b) in Supplement 1). The temporal evolution of the electronic system in the near-single-cycle laser waveform is obtained by solving the time-dependent Schrödinger equation [46]; see Supplement 1 for details. We confirm that the results of the simulations are robust against substantial variations of the parameters, as long as the system breaks the inversion symmetry and the electrons of VB1 are populated mostly around atom B. The results are also robust against the relaxation and dephasing effects; see Supplement 1.

Figure 3(f) shows results for $\varphi_{CE} = 0$ and π. The spectrum for the cosine-shaped single-cycle driving pulse with peak field toward atom B (Se) is smooth (solid line) while the spectrum for the minus-cosine single-cycle pulse with peak field toward atom A (Ga) has harmonic orders with dips in between (dashed line). The time-dependent nonlinear polarizations [see Fig. 3(e)] again show one or two main bursts, similar to the phenomenological picture above [compared with Fig. 3(b)]. However, the quantum-mechanical model now links the sign of the optical asymmetry to the position and type of the atoms, providing an atomistic explanation. Generally, the optical response of condensed matter to long-wavelength radiation is predominantly determined by electrons in the highest occupied valence band, here VB1. As shown in Fig. 3(d), the electrons in VB1 are located around atom B, where the potential is asymmetric and less steep toward the direction of the neighboring atom A. We conclude that the direction, orientation, and different electron affinity of the atoms that form a material's chemical bonds are responsible for the sign, magnitude, and shape of the nonlinear optical response to impulsive single-cycle excitation. The atomistic origin of single-cycle nonlinear optics in complex materials is the quantum-mechanical motion of the valence electrons in the potential made up for them by the atomic environment and bonding structure. In ε-GaSe, the time-dependent nonlinear motion of valence electrons around Se is more nonlinear when they are driven toward the shallower side of the potential, toward Ga, and weaker toward the steeper side, away from Ga.

C. Further Experimental Evidence

In order to further verify our conclusions, we report three more experimental investigations. First, we measure spectra at fixed CEP values but for different peak field amplitudes of the driving field. If the field-driven electronic motion along the chemical bonds is dictated by the potential and waveform, the spectral shape of nonlinear output and in particular the absence or appearance of photon-order interferences should not strongly depend on the absolute electric field strength (see also Fig. S5 in Supplement 1). Figures 4(a) and 4(b) show the measured output spectra as a function of excitation intensity for $\varphi_{CE} = 0$ and $\varphi_{CE} = \pi$, respectively. For weaker pump pulses, the harmonic intensities are reduced by up to 3 orders of magnitude, but the general spectral shape with or without harmonic orders remains the same.

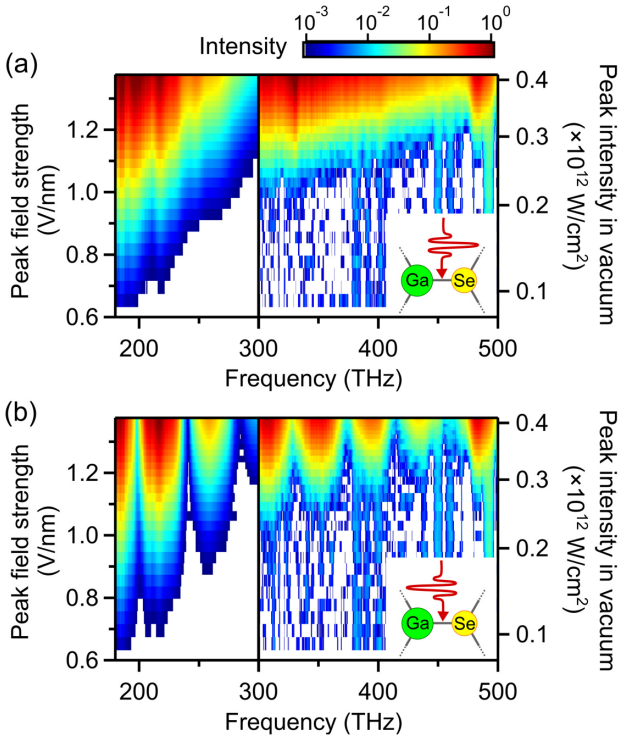

Fig. 4. Dependence on excitation field strength. (a) Output spectrum for cosine excitation as a function of electric peak field strength. (b) Field-strength-dependent output spectrum for minus-cosine excitation. The spectral shape remains the same although the spectral intensities change by more than 3 orders of magnitude.

Second, we report nonlinear emission spectra as a function of crystal angle with respect to laser polarization [θ in Fig. 5(a)]. In the experiment, the crystal is rotated around the c axis. ε-GaSe has a threefold symmetry around the c axis (space group D_3h). It repeats itself every 120°, but opposite Ga–Se bonds occur every 60° [see Fig. 5(a)]. Aiming for reproduction of earlier results [17,39], Fig. 5(d) shows output spectra created with an excitation waveform that is chirped to a duration of 3.8 optical cycles. The harmonic-order interference appears every 60°, although a rotation of 120° is required to reproduce the original atomic structure. A 3.8 cycle excitation field has too many optical cycles and, therefore, averages out in the spectrum the underlying asymmetric response and directivity of the heteronuclear bonds. In other words, Ga–Se and Se–Ga produce the same spectral results, and time-domain metrology is needed to see the differences [17]. In contrast, Figs. 5(b) and 5(c) show the output spectrum as a function of angle for the case of single-cycle excitation fields, again for $\varphi_{CE} = 0$ and π. The 60° periodicity disappears, and instead a 120° periodicity shows up, corresponding to the angle between the three Ga–Se bonds when taking into account the bond direction. Furthermore, when comparing the cosine and minus-cosine results of Figs. 5(b) and 5(c), we see that the whole pattern shifts by 60°. This value reflects the difference of 180° between a cosine and a minus-cosine pulse minus the 120° of the Ga–Se bonds. To our best

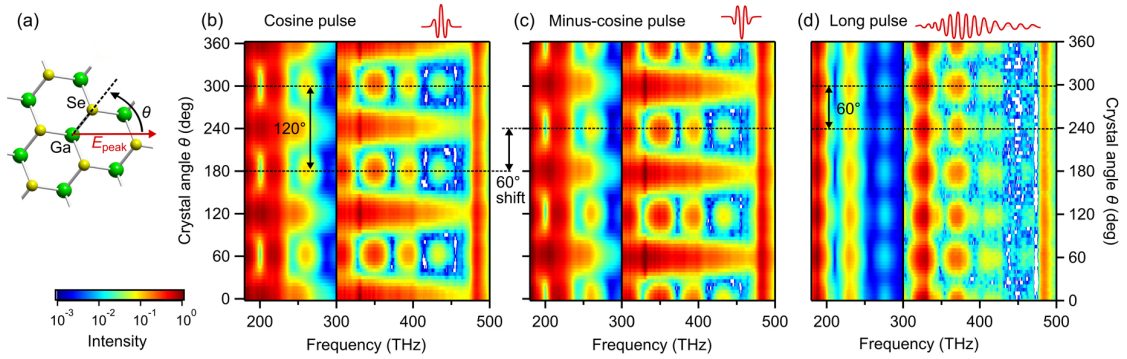

Fig. 5. Scan of crystal angle and absolute bond orientation. (a) Definition of the crystal angle θ between the peak electric field vector direction and the Ga–Se bond direction. (b) Output spectrum as a function of θ for cosine excitation. (c) Output spectrum for minus-cosine pulse. The periodicity of 120° and the shift to each other by 60° reveal the polar chemical bonds. (d) Angle scan with longer chirped pulses (3.8 cycles). Due to the chirp, the spacing between harmonics (46 THz) is larger than that of the single-cycle fields (43 THz) in (b) and (c); see Supplement 1 for details. A periodicity of 60° shows the averaging of the fundamental asymmetric response by the multiple optical cycles.

knowledge, atomic arrangement in a crystal including bond orientation is observed for the first time by purely spectroscopic means [29–32,47]. This is enabled by the impulsive excitation, which drives unidirectional electronic motion on atomic dimensions.

As a third investigation, we repeated all the above measurements with a 55-μm-thick ε-GaSe crystal, twice thicker than the crystal used above. We obtained qualitatively identical results; see Supplement 1 and Fig. S4, demonstrating that all observed phenomena indeed originate from atomic-scale electron dynamics and not from any macroscopic optical pulse propagation or dispersion effects [48–50].

3. CONCLUSION

In combination with the results of Fig. 2, these observations establish and verify an atomistic picture of nonlinear optics on the basis of the chemical bonds and suggest the possibility of exploring the potential energy landscape of asymmetric materials by launching and tracking directional electronic motion via single-cycle mid-infrared excitation. The spectral shape of the nonlinear optical emission is dictated by the field-driven valence electronic dynamics on atomic dimensions and for heteronuclear materials by the orientation, angles, and polarity of the chemical bonds. The absolute direction of the electric field from Ga to Se is relevant for either the production of a broadband, featureless spectrum or a spectrum in form of even and odd harmonics. Our ability to track with highly simplified approximations the characteristics of the emission spectrum back to the real-space physics of single chemical bonds indicates the general applicability of our results for the nonlinear optics of any material without inversion symmetry—for example, oriented molecules in the gas phase [33–35] or materials with multiple types of chemical bonds. Experimentally, single-cycle mid-infrared pulses are useful to launch and control isolated electronic motion in complex networks of chemical bonds in crystals at energies below the bandgap, in order to investigate the atomic structure and binding potentials on picometer dimensions [24], to develop novel materials for nonlinear optics, or to eventually control electronics at the frequency of light [51].

Funding. Ministry of Education, Culture, Sports, Science and Technology (Exploratory Challenge on Post-K Computer, MEXT Q-LEAP JPMXS0118067246); Japan Society for the Promotion of Science (18K14145, 19H00869, 19H02623, JP20H05670); Japan Science and Technology Agency (Center of Innovation Program, CREST JPMJCR15N1, Research and Education Consortium); Munich-Centre for Advanced Photonics; Friedrich-Alexander-Universität Erlangen-Nürnberg (Emerging Talent Initiative); European Research Council (647771).

Acknowledgment. We thank C. Hofer and I. Pupeza for helpful discussions on mid-infrared optics and F. Krausz for generous support and laboratory infrastructure. Y. M. acknowledges P. Hommelhoff for general support.

Disclosures. The authors declare no conflicts of interest.

Supplemental document. See Supplement 1 for supporting content.

†These authors contributed equally to this paper.

REFERENCES

1. R. W. Boyd, *Nonlinear Optics* (Academic, 2008).
2. A. H. Chin, O. G. Calderón, and J. Kono, "Extreme midinfrared nonlinear optics in semiconductors," Phys. Rev. Lett. **86**, 3292–3295 (2001).
3. S. Ghimire and D. A. Reis, "High-harmonic generation from solids," Nat. Phys. **15**, 10–16 (2019).
4. G. Vampa, T. J. Hammond, N. Thiré, B. E. Schmidt, F. Légaré, C. R. McDonald, T. Brabec, and P. B. Corkum, "Linking high harmonics from gases and solids," Nature **522**, 462–464 (2015).
5. N. Yoshikawa, T. Tamaya, and K. Tanaka, "High-harmonic generation in graphene enhanced by elliptically polarized light excitation," Science **356**, 736–738 (2017).
6. S. Han, L. Ortmann, H. Kim, Y. W. Kim, T. Oka, A. Chacon, B. Doran, M. Ciappina, M. Lewenstein, S.-W. Kim, S. Kim, and A. S. Landsman, "Extraction of higher-order nonlinear electronic response in solids using high harmonic generation," Nat. Commun. **10**, 3272 (2019).
7. G. Ndabashimiye, S. Ghimire, M. Wu, D. A. Browne, K. J. Schafer, M. B. Gaarde, and D. A. Reis, "Solid-state harmonics beyond the atomic limit," Nature **534**, 520–523 (2016).
8. Y. Yang, J. Lu, A. Manjavacas, T. S. Luk, H. Liu, K. Kelley, J.-P. Maria, E. L. Runnerstrom, M. B. Sinclair, S. Ghimire, and I. Brener, "High-harmonic generation from an epsilon-near-zero material," Nat. Phys. **15**, 1022–1026 (2019).
9. A. J. Uzan, G. Orenstein, Á. Jiménez-Galán, C. McDonald, R. E. F. Silva, B. D. Bruner, N. D. Klimkin, V. Blanchet, T. Arusi-Parpar, M. Krüger, A. N. Rubtsov, O. Smirnova, M. Ivanov, B. Yan, T. Brabec, and N. Dudovich, "Attosecond spectral singularities in solid-state high-harmonic generation," Nat. Photonics **14**, 183–187 (2020).
10. T. T. Luu, M. Garg, S. Y. Kruchinin, A. Moulet, M. T. Hassan, and E. Goulielmakis, "Extreme ultraviolet high-harmonic spectroscopy of solids," Nature **521**, 498–502 (2015).
11. A. Schiffrin, T. Paasch-Colberg, N. Karpowicz, V. Apalkov, D. Gerster, S. Mühlbrandt, M. Korbman, J. Reichert, M. Schultze, S. Holzner, J. V. Barth, R. Kienberger, R. Ernstorfer, V. S. Yakovlev, M. I. Stockman, and F.

Krausz, "Optical-field-induced current in dielectrics," Nature **493**, 70–74 (2013).
12. M. Schultze, E. M. Bothschafter, A. Sommer, S. Holzner, W. Schweinberger, M. Fiess, M. Hofstetter, R. Kienberger, V. Apalkov, V. S. Yakovlev, M. I. Stockman, and F. Krausz, "Controlling dielectrics with the electric field of light," Nature **493**, 75–78 (2013).
13. T. Higuchi, C. Heide, K. Ullmann, H. B. Weber, and P. Hommelhoff, "Light-field-driven currents in graphene," Nature **550**, 224–228 (2017).
14. H. A. Hafez, S. Kovalev, J. C. Deinert, Z. Mics, B. Green, N. Awari, M. Chen, S. Germanskiy, U. Lehnert, J. Teichert, Z. Wang, K. J. Tielrooij, Z. Liu, Z. Chen, A. Narita, K. Müllen, M. Bonn, M. Gensch, and D. Turchinovich, "Extremely efficient terahertz high-harmonic generation in graphene by hot Dirac fermions," Nature **561**, 507–511 (2018).
15. O. Schubert, M. Hohenleutner, F. Langer, B. Urbanek, C. Lange, U. Huttner, D. Golde, T. Meier, M. Kira, S. W. Koch, and R. Huber, "Sub-cycle control of terahertz high-harmonic generation by dynamical Bloch oscillations," Nat. Photonics **8**, 119–123 (2014).
16. M. Hohenleutner, F. Langer, O. Schubert, M. Knorr, U. Huttner, S. W. Koch, M. Kira, and R. Huber, "Real-time observation of interfering crystal electrons in high-harmonic generation," Nature **523**, 572–575 (2015).
17. F. Langer, M. Hohenleutner, U. Huttner, S. W. Koch, M. Kira, and R. Huber, "Symmetry-controlled temporal structure of high-harmonic carrier fields from a bulk crystal," Nat. Photonics **11**, 227–231 (2017).
18. M. Garg, M. Zhan, T. T. Luu, H. Lakhotia, T. Klostermann, A. Guggenmos, and E. Goulielmakis, "Multi-petahertz electronic metrology," Nature **538**, 359–363 (2016).
19. M. Lucchini, S. A. Sato, J. Herrmann, A. Ludwig, M. Volkov, L. Kasmi, Y. Shinohara, K. Yabana, L. Gallmann, and U. Keller, "Observation of femtosecond dynamical Franz-Keldysh effect in polycrystalline diamond," Science **353**, 916–919 (2016).
20. H. Mashiko, K. Oguri, T. Yamaguchi, A. Suda, and H. Gotoh, "Petahertz optical drive with wide-bandgap semiconductor," Nat. Phys. **12**, 741–745 (2016).
21. M. Volkov, S. A. Sato, F. Schlaepfer, L. Kasmi, N. Hartmann, M. Lucchini, L. Gallmann, A. Rubio, and U. Keller, "Attosecond screening dynamics mediated by electron localization in transition metals," Nat. Phys. **15**, 1145–1149 (2019).
22. G. Vampa, T. J. Hammond, N. Thiré, B. E. Schmidt, F. Légaré, C. R. McDonald, T. Brabec, D. D. Klug, and P. B. Corkum, "All-optical reconstruction of crystal band structure," Phys. Rev. Lett. **115**, 193603 (2015).
23. A. A. Lanin, E. A. Stepanov, A. B. Fedotov, and A. M. Zheltikov, "Mapping the electron band structure by intraband high-harmonic generation in solids," Optica **4**, 516–519 (2017).
24. H. Lakhotia, H. Y. Kim, M. Zhan, S. Hu, S. Meng, and E. Goulielmakis, "Laser picoscopy of valence electrons in solids," Nature **583**, 55–59 (2020).
25. M. T. Hassan, T. T. Luu, A. Moulet, O. Raskazovskaya, P. Zhokhov, M. Garg, N. Karpowicz, A. M. Zheltikov, V. Pervak, F. Krausz, and E. Goulielmakis, "Optical attosecond pulses and tracking the nonlinear response of bound electrons," Nature **530**, 66–70 (2016).
26. H. Liang, P. Krogen, Z. Wang, H. Park, T. Kroh, K. Zawilski, P. Schunemann, J. Moses, L. F. DiMauro, F. X. Kärtner, and K.-H. Hong, "High-energy mid-infrared sub-cycle pulse synthesis from a parametric amplifier," Nat. Commun. **8**, 141 (2017).
27. H. Shirai, F. Kumaki, Y. Nomura, and T. Fuji, "High-harmonic generation in solids driven by subcycle midinfrared pulses from two-color filamentation," Opt. Lett. **43**, 2094–2097 (2018).
28. P. B. Corkum and F. Krausz, "Attosecond science," Nat. Phys. **3**, 381–387 (2007).
29. N. Kumar, S. Najmaei, Q. Cui, F. Ceballos, P. M. Ajayan, J. Lou, and H. Zhao, "Second harmonic microscopy of monolayer MoS_2," Phys. Rev. B **87**, 161403 (2013).
30. L. M. Malard, T. V. Alencar, A. P. M. Barboza, K. F. Mak, and A. M. de Paula, "Observation of intense second harmonic generation from MoS_2 atomic crystals," Phys. Rev. B **87**, 201401 (2013).
31. Y. Li, Y. Rao, K. F. Mak, Y. You, S. Wang, C. R. Dean, and T. F. Heinz, "Probing symmetry properties of few-layer MoS_2 and h-BN by optical second-harmonic generation," Nano Lett. **13**, 3329–3333 (2013).
32. H. Liu, Y. Li, Y. S. You, S. Ghimire, T. F. Heinz, and D. A. Reis, "High-harmonic generation from an atomically thin semiconductor," Nat. Phys. **13**, 262–265 (2017).
33. E. Frumker, C. T. Hebeisen, N. Kajumba, J. B. Bertrand, H. J. Wörner, M. Spanner, D. M. Villeneuve, A. Naumov, and P. B. Corkum, "Oriented rotational wave-packet dynamics studies via high harmonic generation," Phys. Rev. Lett. **109**, 113901 (2012).
34. E. Frumker, N. Kajumba, J. B. Bertrand, H. J. Wörner, C. T. Hebeisen, P. Hockett, M. Spanner, S. Patchkovskii, G. G. Paulus, D. M. Villeneuve, A. Naumov, and P. B. Corkum, "Probing polar molecules with high harmonic spectroscopy," Phys. Rev. Lett. **109**, 233904 (2012).
35. P. M. Kraus, A. Rupenyan, and H. J. Wörner, "High-harmonic spectroscopy of oriented OCS molecules: emission of even and odd harmonics," Phys. Rev. Lett. **109**, 233903 (2012).
36. B.-H. Chen, E. Wittmann, Y. Morimoto, P. Baum, and E. Riedle, "Octave-spanning single-cycle middle-infrared generation through optical parametric amplification in $LiGaS_2$," Opt. Express **27**, 21306–21318 (2019).
37. N. Kuroda, O. Ueno, and Y. Nishina, "Lattice-dynamical and photoelastic properties of GaSe under high pressures studied by Raman scattering and electronic susceptibility," Phys. Rev. B **35**, 3860–3870 (1987).
38. K. R. Allakhverdiev, M. Ö. Yetis, S. Özbek, T. K. Baykara, and E. Y. Salaev, "Effective nonlinear GaSe crystal. Optical properties and applications," Laser Phys. **19**, 1092–1104 (2009).
39. K. Kaneshima, Y. Shinohara, K. Takeuchi, N. Ishii, K. Imasaka, T. Kaji, S. Ashihara, K. L. Ishikawa, and J. Itatani, "Polarization-resolved study of high harmonics from bulk semiconductors," Phys. Rev. Lett. **120**, 243903 (2018).
40. U. Huttner, M. Kira, and S. W. Koch, "Ultrahigh off-resonant field effects in semiconductors," Laser Photon. Rev. **11**, 1700049 (2017).
41. I. Floss, C. Lemell, G. Wachter, V. Smejkal, S. A. Sato, X.-M. Tong, K. Yabana, and J. Burgdörfer, "*Ab initio* multiscale simulation of high-order harmonic generation in solids," Phys. Rev. A **97**, 011401 (2018).
42. T. Otobe, "First-principle description for the high-harmonic generation in a diamond by intense short laser pulse," J. Appl. Phys. **111**, 093112 (2012).
43. N. Tancogne-Dejean, O. D. Mücke, F. X. Kärtner, and A. Rubio, "Impact of the electronic band structure in high-harmonic generation spectra of solids," Phys. Rev. Lett. **118**, 087403 (2017).
44. E. Mooser, I. C. Schlüter, and M. Schlüter, "The electronic charge densities in semiconducting layer and chain structures," J. Phys. Chem. Solids **35**, 1269–1284 (1974).
45. D. V. Rybkovskiy, A. V. Osadchy, and E. D. Obraztsova, "Transition from parabolic to ring-shaped valence band maximum in few-layer GaS, GaSe, and InSe," Phys. Rev. B **90**, 235302 (2014).
46. T. Ikemachi, Y. Shinohara, T. Sato, J. Yumoto, M. Kuwata-Gonokami, and K. L. Ishikawa, "Trajectory analysis of high-order-harmonic generation from periodic crystals," Phys. Rev. A **95**, 043416 (2017).
47. Y. S. You, D. A. Reis, and S. Ghimire, "Anisotropic high-harmonic generation in bulk crystals," Nat. Phys. **13**, 345–349 (2016).
48. A. Kiyama, J. I. R. O. I. Tatani, and N. O. I. Shii, "Nonlinear propagation effects in high harmonic generation in reflection and transmission from gallium arsenide," Opt. Express **26**, 29393–29400 (2018).
49. J. Lu, E. F. Cunningham, Y. S. You, D. A. Reis, and S. Ghimire, "Interferometry of dipole phase in high harmonics from solids," Nat. Photonics **13**, 96–100 (2019).
50. G. Vampa, Y. S. You, H. Liu, S. Ghimire, and D. A. Reis, "Observation of backward high-harmonic emission from solids," Opt. Express **26**, 12210–12218 (2018).
51. F. Krausz and M. I. Stockman, "Attosecond metrology: from electron capture to future signal processing," Nat. Photonics **8**, 205–213 (2014).